Synthesis of magnetic Fe and Co nano-whiskers and platelets via physical vapor deposition

Wenting Huang [a,b], Christophe Gatel [c], Zi-An Li [d], Gunther Richter [b,*]

[a] Institute for Applied Materials, Karlsruhe Institute of Technology, Hermann-von Helmholtz-Platz 1, 76344 Eggenstein-Leopoldshafen, Germany
[b] Max Planck Institute for Intelligent Systems, Heisenbergstr. 3, 70569 Stuttgart, Germany
[c] CEMES-CNRS, 29 rue J. Marvig, BP4347, 31055 Toulouse, France
[d] Ernst Ruska-Centre for Microscopy and Spectroscopy with Electrons and Peter Grünberg Institute, Forschungszentrum Jülich, 52425 Jülich, Germany

HIGHLIGHTS

- Freestanding nanowhisker grow for BCC Fe, FCC Co and HCP Co.
- Nanowhiskers are always magnetized along the whisker axes.
- Only single magnetic domain structures are seen by electron holography.
- Observations are consistent with magnetic energy density considerations.

GRAPHICAL ABSTRACT
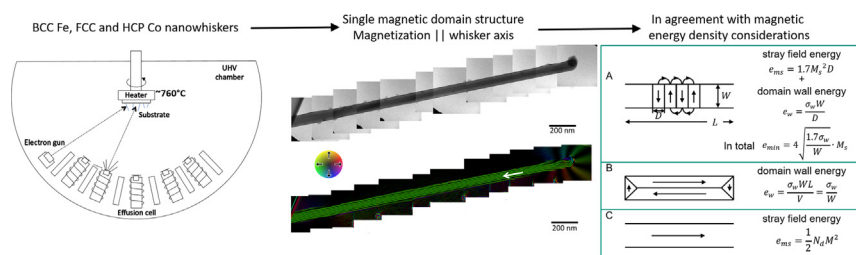
ABSTRACT

Fe and Co nano-whiskers and Co platelets were synthesized via physical vapor deposition without any template and catalyst. Transmission electron microscopic analyses revealed that the Fe whiskers were all single crystal with whisker axis along [1 0 0] crystallographic direction. Both FCC and HCP crystal structures were found in the Co whiskers with stacking faults and micro-twins. Off-axis Electron holography results showed that all the whiskers synthesized were magnetic single domain structures. Vortex state was observed in a small platelet of high symmetry.

© 2021 The Authors. Published by Elsevier Ltd. This is an open access article under the CC BY-NC-ND license (http://creativecommons.org/licenses/by-nc-nd/4.0/).

1. Introduction

Nanowires are promising building blocks of novel nanodevices thanks to their physical, chemical and material properties. As their size becomes smaller, the electrical conductivity decreases [1], and mechanical strength increases [2–4]. This is often attributed to the increasing surface to volume ratio, extra internal interfaces and other deviations from bulk crystals. Modern applications of nanostructures often rely on one or more of those properties. Sensor [5] or actuators [6] rely often on the changes in e.g. resistance or piezoelectricity as a function of mechanical loading. The propagation and steering of nano- and microrobots on the other hand is facilitated by application of magnetic thin films and nanoparticles [7,8]. It is well known that magnetic domain structure is also influenced by the overall geometry of the devices. Smaller dimensions lead typically to single magnetic domain structures.

Magnetic whiskers, or wires, have been successfully prepared via different methods, such as reduction of halides [9,10], electrodeposition with porous anodic alumina templates [11,12], and decomposition of perovskite [13], etc.. Reduction of halides results in whiskers with diameters of several micrometers [9,14] and are not electron transparent. Template based methods [15] produce nanowires with magnetization direction parallel to their structure axis. However, these nanowires are prone to defect incorporation

* Corresponding author.
  E-mail address: richter@is.mpg.de (G. Richter).

in their bulk and on the surfaces [16]. Moreover, their cross-section are determined by the pores, which results in non-thermodynamically equilibrium surface crystallography. Decomposition of perovskites is used to synthesize freestanding ferromagnetic wires, but is limited by the choice of materials. Additionally, due to the process, the surface is roughened by the process [13]. As such, it is difficult to rule out contributions from defects when considering the reported magnetic properties of the nanowires prepared by these methods.

A further challenge for applications is to combine different materials in a single structure. Bamboo structures can be grown by changing the sequence of materials during fabrication [17,18]. Layered or core–shell structures are fabricated by growing a second material on the surfaces of the first one [19]. Again, control of defects and surface quality is desired to separate genuine physical material parameters from effects introduced from the fabrication processes.

Nano-whiskers have been proven to be defect-scarce and with perfect surface facets [3,20,21]. No dislocations, especially no axial screw dislocations are found in the Au, Ag and Cu whiskers grown by physical vapor deposition. No grain boundaries are observed for pristine whiskers, with high quality symmetrical tilt grain boundaries introduced only beyond the predicted theoretical strength via propagation of Schockley partial dislocations [20,22]. The cross-section of the whiskers are determined by the thermodynamic minimum energy configuration and surface facets which are predicted by the Wulff shape. The crystallographic quality of the facets is high which allows for heteroepitaxial growth at room temperature [21,23]. Therefore, thanks to the absence of structural defects and chemical impurities, single crystal whiskers synthesized with physical vapor deposition with perfect facets are ideal for investigating the magnetic properties of transition metals (Fe and Co) without the potential influence of any defects. Theoretical limits of the magnetic properties may be reached with such materials [24,25]. The investigation of individual ferromagnetic nanowhisker is of interest, because it establishes a base line for the magnetic properties before device integration. Research interest on the magnetic properties of transition metal whiskers are also stimulated by their potential applications. The high magnetic shape anisotropy and high coercivity attributed from the large aspect ratio make whiskers particularly interesting for ultra-high-density magnetic recording system [26]; hyperthermia cancer treatment [27]; magnetic nanowire–enhanced opto-magnetic tweezers [28]; electro-drive actuators [29].

Micro-sized Fe whiskers [10,30] were reported to be multi-domain structures magnetized along the direction of the magnetocrystalline easy axes. The magnetic coercive force was found close to the theoretic value. The coercivity increases with decreasing whisker diameter. The whiskers even exhibit a single domain structure when the diameter is small enough. A strong magnetic anisotropy along the whisker axis was reported in single crystal Ni nanowires (with ⟨1 0 0⟩ and ⟨1 1 1⟩ as the axial directions), as well as in Co and Fe nanowire, regardless of the crystallographic orientation [11,13]. The shape anisotropy of the nanowires and the dipolar interactions between them dominates over the other magnetic contributions (e.g. magnetocrystalline anisotropy).

The aforementioned previous studies for nanosized wires are always limited by the quality of the investigated structures. Therefore, it is worthwhile to investigate defect-scarce nano-whiskers with perfect bulk and surface crystal structure to differentiate between genuine size effects and possible defect influences.

In the case of whiskers, it is assumed that the magnetic easy axis (as result of balance between magnetocrystalline anisotropy and shape anisotropy) to be either perpendicular or parallel to the whisker axis. This reduces the possible domain configurations to only three (Fig. 1), based on Kittel's models [25]. For the sake of

simplicity, the magneto-striction effects are neglected. The cross section of the whiskers is further assumed to be square shape with width W.

Fig. 1-a shows the case where the magnetocrystalline easy axis is perpendicular to the whisker axis and when the magnetocrystalline anisotropy overrules the shape anisotropy. In this case, a multi-domain structure with antiparallel up and down domains of thickness D is formed. Including the saturation magnetization M_s, the magnetostatic energy per unit area can be assumed as

$$e_{ms} = 2 \times 0.85 M_s^2 D = 1.7 M_s^2 D. \tag{1}$$

The factor of 2 arises from the fact that two surfaces have to be taken into account [31]. The domain wall energy per unit area is

$$e_w = \frac{\sigma_w W}{D}. \tag{2}$$

where σ_w is energy per unit area of a domain wall. The total energy per unit area is minimal when

$$D = \sqrt{\frac{\sigma_w W}{1.7 M_s^2}}. \tag{3}$$

At which point the (minimum) energy per unit surface area becomes

$$e_{min} = 2\sqrt{1.7\sigma_w W} \cdot M_s. \tag{4}$$

The corresponding minimum energy per volume is

$$e_{min} = \frac{2\sqrt{1.7\sigma_w W} \cdot M_s \times 2LW}{LW^2} = 4\sqrt{\frac{1.7\sigma_w}{W}} \cdot M_s. \tag{5}$$

For the configuration shown in Fig. 1b, the whisker is composed of two elongated domains with the flux circuit being closed internally by triangular caps. The magnetostatic energy in this case is zero. Only the domain wall energy needs to be taken into account. Considering only the larger contribution from the 180° domain walls parallel to the whisker axis, the domain wall energy per volume is

$$e_w = \frac{\sigma_w W L}{V} = \frac{\sigma_w}{W}. \tag{6}$$

Finally, for the configuration shown in Fig. 1c, the whisker consists of only one domain magnetized along the whisker axis. Only the magnetostatic energy needs to be considered. With magnetization M, its volume density is

$$e_{ms} = \frac{1}{2} N_d M^2. \tag{7}$$

The demagnetizing coefficient N_d is equal to a prolate spheroid with the same aspect ratio [32].

The aim of the paper is the analysis of the magnetic domain structure in ferromagnetic nanowires via electron holography. The experimental results are connected to theoretical predictions derived from basic magnetic energy density considerations. It is evidenced, that even for materials where the crystallographic orientation of the bulk easy axis is not parallel to the axial direction of nanowires, the occurrence of a single magnetic domain without domain boundaries can be described and predicted in the framework of the minimization of the energy density.

2. Experimental methods

The magnetic nanostructures were prepared by physical vapor deposition in an ultra-high vacuum (UHV) Molecular Beam Epitaxy (MBE, DCA Instruments, Finland) system with a base pressure of under 2×10^{-10} mbar. W and Mo wires with diameters of 0.45 μm were used as substrates without any prior treatments or
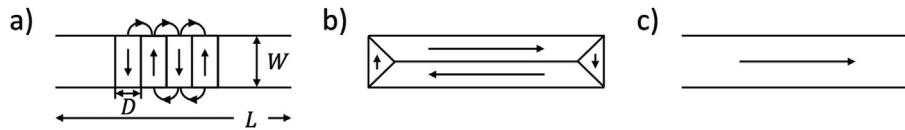
Fig. 1. Possible domain configurations in a whisker.

preparations, as the growth of the whiskers has been expected to be aided by impurities and defects on the surface. For both Fe and Co whiskers, the substrates were heated up to 760 °C to ensure sufficient surface diffusion, which is critical for the nucleation and subsequent growth of the whiskers. The deposition rate was controlled at R = 0.05 nm/s and was monitored with a quartz balance. Rotation of the specimen plate around its surface normal was applied during the entire processes in order to improve the homogeneity of the deposition.

After the deposition, the specimens were cooled down to RT and subsequently retrieved from the UHV system for further analysis. The morphology and the crystallography of the nanostructures were studied with scanning electron microscopy (SEM, LEO 1530VP Gemini) and transmission electron microscopy (TEM, Philips CM200 and JEOL ARM1250). The magnetic domain structures were studied using off-axis electron holography (Hitachi HF3300C-I2TEM).

For TEM sample preparation, nanostructures (mostly whiskers) were transferred to a standard 300-mesh TEM grid by scratching the coated substrate surface. The grids were covered with lacy or holey C-film for supporting the nanostructures. Lamellae specimens of the cross-section of the whisker were also prepared by Focused Ion Beam (FIB, FEI Dual-Beam), in order to inspect the cross-sectional microstructures.

3. Results and discussions

3.1. Co whiskers

After growth (Fig. 2), the entire surface of the Mo wire was full of Co objects (whiskers platelets and particles) as shown in Fig. 2-a

whereas on the W wire surface only a few long whiskers were observed (Fig. 2-b). The result can be explained by the different surface conditions of the two wires, including the density of defects and impurities, the wettability of Co related to the interface energy as well as the mobility of Co atoms on Mo and W surfaces. Co tends to follow Frank–van der Merwe growth mode on W surfaces [33] while a Stranski–Krastanov mode on Mo surfaces has been observed [34]. Phase transformation of Co (from FCC to HCP, ~ 430 °C) is expected when cooling down the Co whiskers from their growth temperature (~760 °C) to RT for further investigations. The growth temperature is above the HCP – FCC phase transformation but below the Curie temperature. Both HCP and FCC crystal structures were identified in the Co whiskers by electron diffraction. A Co whisker with FCC structure is shown in Fig. 2-c. The whisker axis is along the $\langle 1\,1\,0 \rangle$ direction as indexed in the electron diffraction pattern (inset). Fig. 2-d shows an HCP Co whisker from the [0 0 0 1] zone axis. The axial direction of the whisker in this case is parallel to the $\langle 1\,2\,1\,0 \rangle$ direction. The cross section of Co whiskers was usually a pentagon with size ranging from 20 to 300 nm, while the length of the whiskers was from 2 to 100 μm. More details about the crystal structures of Co whiskers will be discussed in a separate paper.

3.2. Fe whiskers

Fe whiskers were obtained also on Mo and W wires (Fig. 3-a), as well as on SrTiO₃(0 0 1) (STO) substrates with a mediating TiC layer (Fig. 3-b). The growth temperature was about 760 °C for the Fe whiskers grown on Mo or W wires and about 810 °C for those grown on STO substrates. The substrate temperature for Mo and W wires was close to, for STO higher than the Fe Curie tempera-
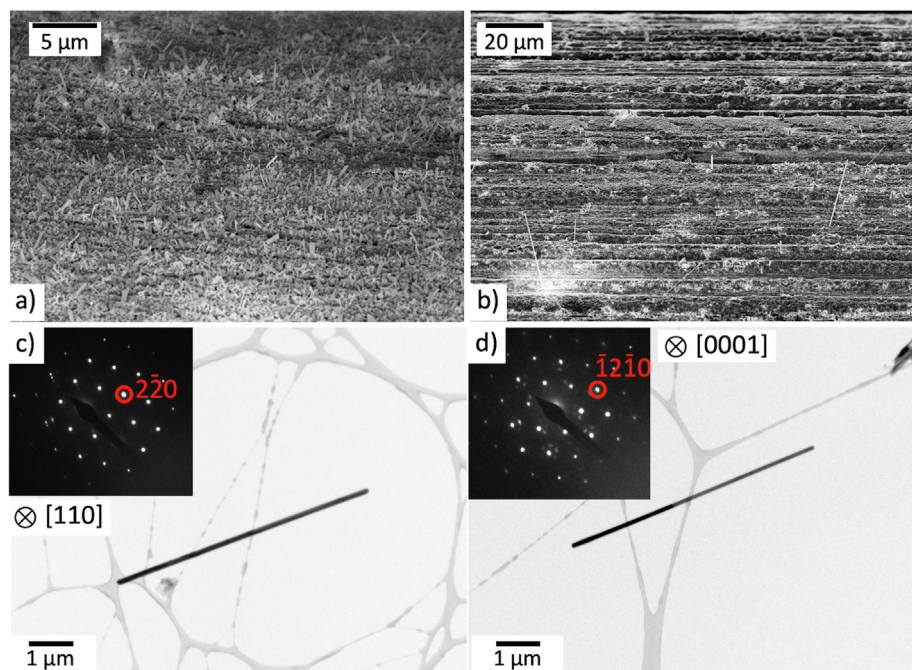

Fig. 2. SEM micrographs of the surface of (a) a Mo and (b) a W wire after 180 nm (nominal value) of Co deposition at 760 °C. TEM micrograph and (inset) corresponding diffraction pattern of Co whiskers with a (c) FCC and a (d) HCP structure.

ture. The morphology of the objects after growth also depends on the type of the substrate. As shown in Fig. 3, the Fe whiskers grown on the Mo wire resemble the Co whiskers grown on the same substrate. The axial crystal orientation of the whiskers was fixed but their relative orientation to the substrate surface was completely random. This is in contrast to what was obtained on STO substrates where whiskers with two preferential orientations relative to the substrate were observed. Careful analysis revealed that the two growth directions were in fact perpendicular to one another. This can be understood as due to the 4-fold symmetry of the (0 0 1) STO substrate. Indeed, since the mediating TiC layer was mostly amorphous, the growth direction of the Fe whiskers can only be inherited from the underlying STO substrate. This implies that the mediating layer in this case merely provided the preferred nucleation sites (defects, possibly as vacancies or holes) for the whisker growth, and that an epitaxial relationship was possibly established between the Fe whiskers and the STO substrate. The dimensions of Fe whiskers were pretty much the same as the Co whisker, as cross-sectional size varied from 20 to 300 nm, the length differed from 2 to 100 μm.

Further microscopic analysis on the cross-sectional lamellae (Fig. 3-c and -e) indicated that the cross sections of the Fe whiskers were all rectangular shaped albeit with different aspect ratios. The cross-sectional planes, cut with FIB, were perpendicular to the axial direction of the whiskers, which is the [1 0 0] crystallographic direction of BCC α-Fe. A high resolution HAADF image is shown in Fig. 3-d: the monocrystalline Fe core of the whisker is surrounded by a 3 nm thick oxide layer . Two sets of spots were thus found in the corresponding FFT pattern (inset), one (red circles) corresponds to the (0 0 1) plane of BCC Fe and the other (yellow circles) corresponds to the (0 1 1) plane of FCC Fe_3O_4 or γ-Fe_2O_3. It can also be inferred from the FFT pattern that the sidewalls of the Fe whiskers were composed of 4 crystal planes of the {1 0 0} family. These are

the planes with the lowest surface energy [35]. Finally, it is possible to derive the epitaxial relationship between the BCC Fe whisker and the FCC oxide layer by combining all the above data. The result, $(0\ 1\ 0)_{oxide}\|(1\ 0\ 0)_{Fe}$ and $\langle 0\ 1\ 1\rangle_{oxide}\|\langle 1\ 0\ 0\rangle_{Fe}$, is consistent with what was reported by Wagner [36] and Stockbridge [37] on large single crystals Fe at various temperatures, and by Luborsky [38] on sub-micron Fe whiskers. The oxide thickness is well below 5 nm which is remarkable since the whiskers were stored under ambient atmosphere, and the bulk Fe is prone to oxidation.

Overall, the growth process for nano-whiskers is not fully understood, despite its high reproducibility. The historical explanations based on the incorporation of a screw-dislocation parallel to the whisker axis cannot be confirmed by the microstructural observations in this work. More specifically, the atomistic growth process is still elusive. Growing whisker under UHV conditions minimizes the effect of impurities, which allows geometrical shape influence on physical properties to be studied on purely genuine materials.

3.3. Magnetic domain structures

The Fe and Co whiskers synthesized in this work all have perfect crystal facets with clean and smooth surfaces. These whiskers are the ideal samples for studying the magnetic properties of materials, as they are not affected by incoherent grain boundaries (excluding twin boundaries) or impurities. The peculiar geometry of the whiskers and platelets also provides a unique perspective to the understanding of size related properties in magnetic structures. Whiskers and platelets of Fe and Co were studied with electron holography at room temperature under zero-field conditions. For each measurement, a second hologram was recorded with the specimen inverted, in order to separate the mean inner potential (MIP) with the magnetic field (MAG) contributions in the total
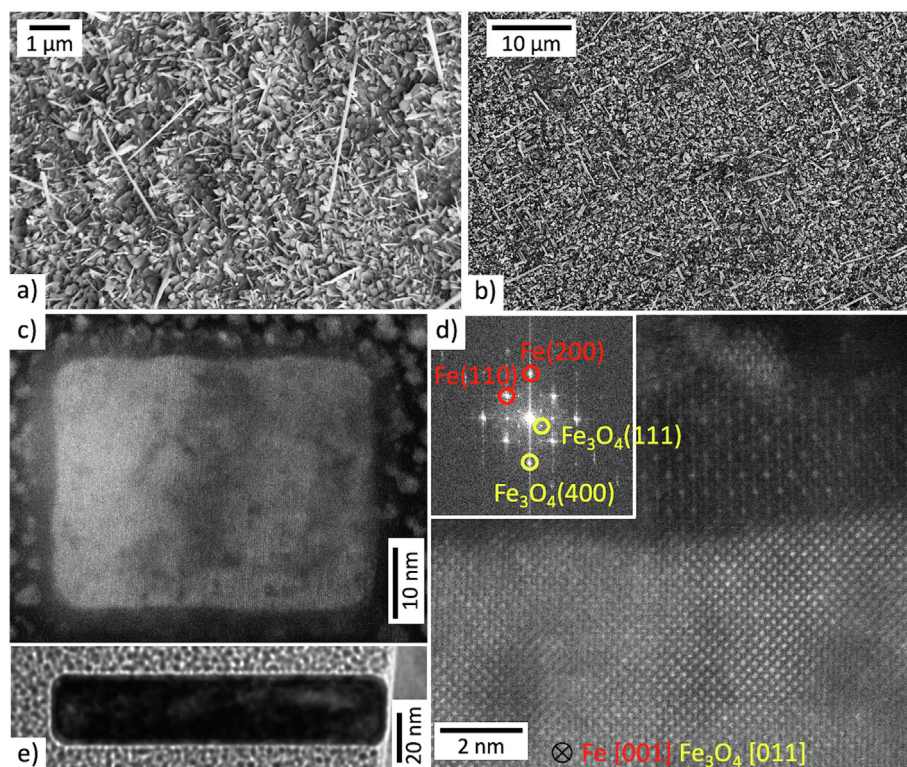

Fig. 3. SEM micrographs of Fe whiskers grown on (a) Mo wire at 760 °C and on (b) STO substrate at 810 °C after 180 nm (nominal value) of Fe deposition. A TiC mediating layer was deposited on the surface of the STO substrates prior to the Fe deposition. (c) STEM image on the cross section of a Fe whisker grown on a W wire, after 180 nm (nominal value) of Fe deposition at 760 °C. (d) HAADF image on the same cross section together with (inset) the corresponding FFT pattern. (e) TEM BF image on the cross section of another Fe whisker grown on the same substrate.

phase shift. A reference hologram was also recorded in vacuum for each measurement for the correction of instrumental and experimental artifacts.

Fig. 4 shows the electron holography results of a Co whisker. The morphology of the whisker can be visualized in the amplitude image (Fig. 4-a). The whisker has a uniform diameter of about 90 ± 2 nm. Fig. 4-b is the MAG phase shift image. The so-called wrapped phase, calculated as the modulo of 2π, is indicated by the false color scale. The outline of the whisker is clearly distinguishable on the phase shift image. The MAG phase shift was along the direction perpendicular to the whisker axis, indicating that the magnetization was along the direction of the whisker axis. A phase-unwrapping algorithm was later applied to remove the discontinuities in the wrapped phase. The contour map (Fig. 4-c) generated from the unwrapped MAG contribution shows the remnant magnetic state of the whisker, which allows for quantitative analysis of the strength and direction of the local flux. The contour lines were homogeneously distributed within the whisker. Their density is proportional to the in-plane component of the induction of the specimen integrated along the electron beam direction. Fig. 4-d shows the magnetic flux lines, the direction of the measured magnetic induction being represented according to the color wheel. The flux lines within the whisker are parallel to the sidewall showing the magnetization direction of the whisker along the whisker axis, as pointed out by the white arrow on the image. No disturbance from domain wall was observed, indicating a single domain structure inside the Co whisker. It is worth to mention, that the magnetization direction of the Co nano-whiskers is always parallel to the whisker axis. The easy magnetization directions are inclined relative to the whisker axis for both FCC and HCP crystal structures.

Fig. 5 shows the holography results on a Fe whisker. The diameter of the whisker is 70 ± 2 nm. The montage of the 12 holograms covers a total 2.2 ± 0.05 μm of the 6.25 ± 0.05 μm long whisker. For BCC Fe whiskers, the whisker axis coincides with the crystal easy axis, along the $\langle 0\,0\,1 \rangle$ direction. The whiskers were randomly distributed on the TEM grids, with enough separation between them to be considered each as an isolated object. Regardless of the magnetostriction effects, the energy density of the three previous described different magnetization configurations can be calculated for Fe with $M_s = 1.714 \times 10^6$ A/m [39] and $\sigma_{w,Fe}^{180} = 2 \times 10^{-3}$ J/m^2 [40], the latter being the specific energy of the (1 0 0)-180° wall. The aspect ratio of the Fe whisker is $c/a \approx 90$. This gives a demagnetization coefficient of $N_d = 0.00528$ [41]. For a multi-domain structure with magnetization perpendicular to the whisker axis, the minimum energy density is calculated as (see Eqs. (3)–(7))

$$e_{min} = 4\sqrt{\frac{1.7\sigma_w}{W}} \cdot M_s = 4.778 \times 10^5 \text{J/m}^3, \tag{8}$$

with a domain size of $D = \sqrt{\frac{\sigma_w W}{1.7 M_s^2}} = 16.7$ nm (see Equ. (3)).

The energy density of a two-domain structure with magnetization parallel to the whisker axis is

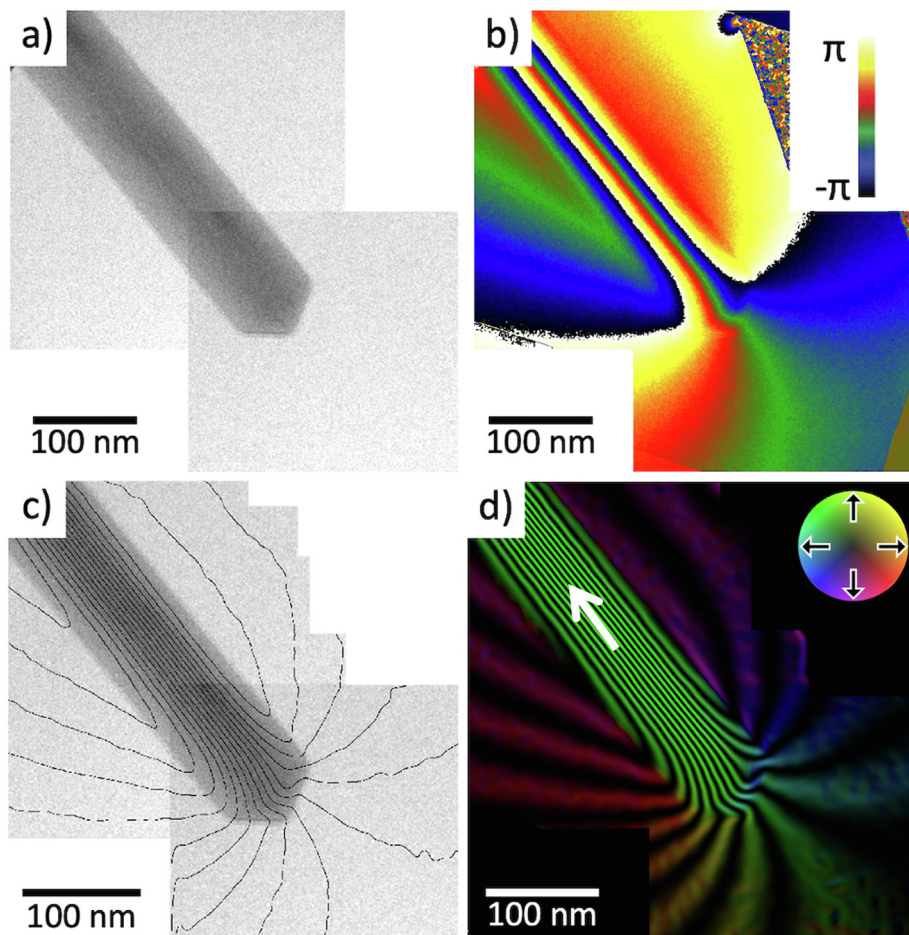$$e_w = \frac{\sigma_w}{W} = 2.8 \times 10^4 \text{ J/m}^3. \tag{9}$$

Fig. 4. Electron holography results on a Co whisker: (a) amplitude image; (b) MAG phase shift; (c) MAG phase contour overlaid with the amplitude image showing the in plane magnetic induction, the spacing of the contour is 0.75 rad; (d) Magnetic flux lines calculated as the cosine of 7 times the MAG contribution to the measured phase shift. The direction of the measured magnetic induction is indicated according to the color wheel and the magnetization direction of the whisker is pointed out by the white arrow.
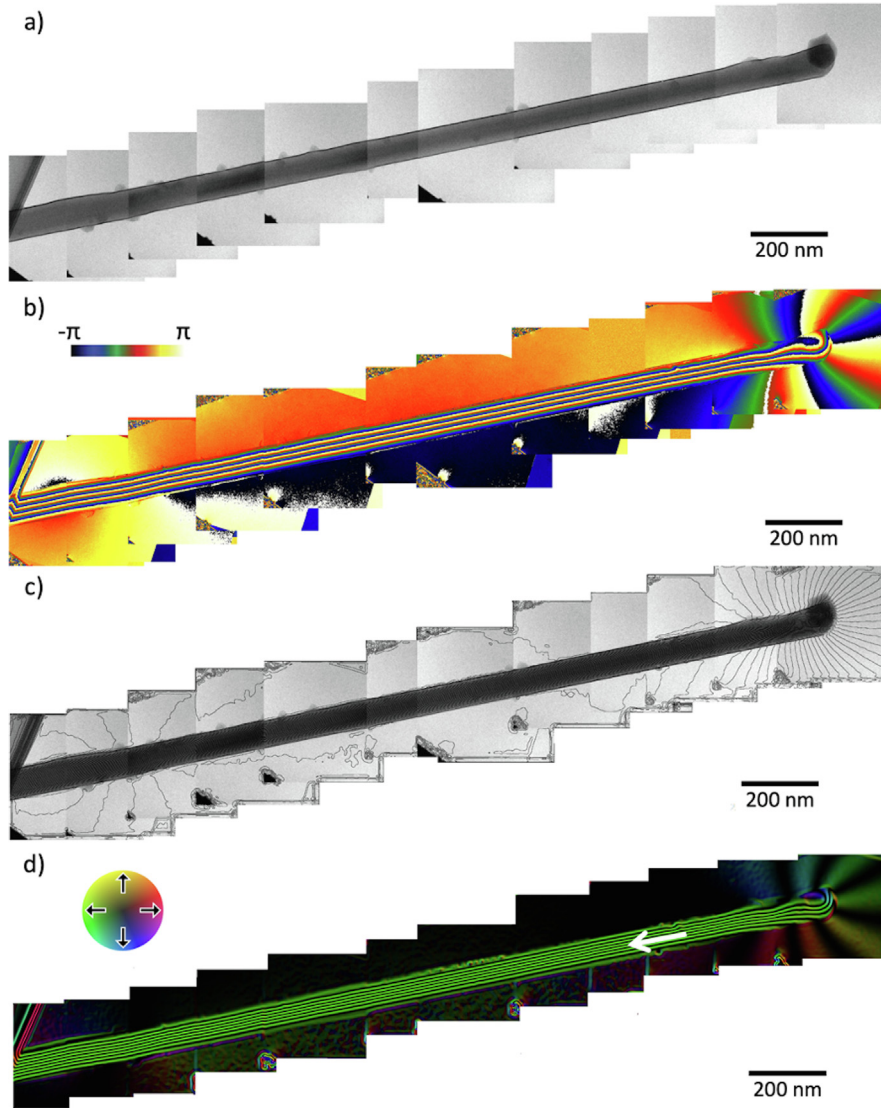
Fig. 5. Electron holography results of a Fe whisker: (a) amplitude image; (b) MAG phase shift; (c) MAG phase contour overlaid with the amplitude image showing the in plane magnetic induction, the spacing of the contour is 0.49 rad; (d) Magnetic flux lines calculated as the cosine of 2 times the MAG contribution to the measured phase shift. The direction of the measured magnetic induction is indicated according to the color wheel and the magnetization direction of the whisker is pointed out by the white arrow.

At last, the energy density of a single domain structure at saturation magnetization writes

$$e_{ms} = \frac{1}{2} N_d M_s^2 = 7.756 \times 10^2 \text{ J/m}^3. \tag{10}$$

It is obvious from the comparison that single domain is energetically the most favorable structure for Fe whiskers of high aspect ratio.

Next, this conclusion is applied to the FCC Co whiskers. The easy axis is along the $\langle 1\,1\,1 \rangle$ direction while their whisker axis is along the $\langle 0\,1\,1 \rangle$ direction. With $M_s = 1.445 \times 10^6$ A/m, the exchange stiffness constant $A = 3.0 \times 10^{-11}$ J/m [42–44] and the anisotropy constants $K_1 = -5.7 \times 10^4$ J/m^3, $K_2 = 1.3 \times 10^4$ J/m^3 [45], the specific domain wall energy $\sigma_{w,Co}^{180} = 2\sqrt{AK_1} = 2.6 \times 10^{-3}$J/m^2 is obtained. Taking the same aspect ratio as 50 and the corresponding demagnetization coefficient $N_d = 0.0094$ as before, the minimum energy density for the multi-domain structure with magnetization perpendicular to the whisker axis is calculated as

$$e_{min} = 4\sqrt{\frac{1.7\sigma_w}{W}} \cdot M_s = 3.84 \times 10^5 \text{ J/m}^3, \tag{11}$$

with a domain size of $D = \sqrt{\frac{\sigma_w W}{1.7 M_s^2}} = 27.1$ nm (see Equ. (3)).

The energy density of a two-domain structure with magnetization parallel to the whisker axis is

$$e_w = \frac{\sigma_w}{W} = 2.6 \times 10^4 \text{J/m}^3. \tag{12}$$

At last, the energy density of a single domain structure at saturation magnetization writes

$$e_{ms} = \frac{1}{2} N_d M_s^2 = 9.81 \times 10^2 \text{J/m}^3. \tag{13}$$

The extra energy density costs from magnetocrystalline anisotropy is calculated as

$$\Delta e_{mc} = e_{mc(110)} - e_{mc(111)} = K_0 + \frac{K_1}{4} - (K_0 + \frac{K_1}{3} + \frac{K_2}{27})$$
$$= 4.27 \times 10^3 \text{J/m}^3. \tag{14}$$

Even with this extra energy density cost, the single domain structure is still the lowest free energy state among the three domain structures considering the dimensions of the whiskers.

The gain in energy is sufficient to orient the magnetization direction parallel to the whisker axis even if the whisker axis is not the easy axis of the material.

Regarding the HCP Co whiskers, the uniaxial symmetry of the HCP lattice initially caused a large magnetocrystalline anisotropy. However, for whiskers with very high aspect ratios, the shape anisotropy becomes predominant which forces the magnetization to align with the whisker axis. Hubert and Schäfer [32] calculated the critical value of the aspect ratio to be 3.5, at which point the shape anisotropy constant becomes comparable to the crystal anisotropy constant with $K_s \approx K_1 = 4.5 \times 10^5$ J/m^3. The HCP Co whiskers synthesized in this study showed aspect ratio much higher than 3.5, thus it is not unexpected that the whiskers were magnetized along the whisker axis due to the predominant shape anisotropy.

The situation is different for platelets with higher symmetry. The electron holography results on a Co platelet are shown in Fig. 6. The platelet is a truncated-triangle with a 3-fold symmetry as can be inferred from the amplitude image (Fig. 6-a). The average length of the three longer sides is 150 ± 4 nm. The vortex state observed in the MAG phase shift image (Fig. 6-b) is understood as due to the high symmetrical shape of the platelet. Larger phase shift is obtained as one moves towards the center of the platelet. The phase shift is well confined within the platelet (since the vortex state is a stray field free or flux closure state), with only a few weak phase shift detected outside the platelet area. The induction lines (Fig. 6-c) and the magnetic flux lines (Fig. 6-d) indicate the presence of a magnetic vortex in the platelet. With the absence of external field, the center of the vortex lies on the central point of the rotational symmetry of the platelet. The vortex state was stabilized by the "round" truncated edges. The sharp angles of the triangle are not favorable for the vortex state due to the high exchange energy [46].

For large platelets that are not highly symmetric, multi-domain structures were observed instead. Fig. 7 shows the Lorentz microscope image of such a platelet. The Co platelet exhibited a closure
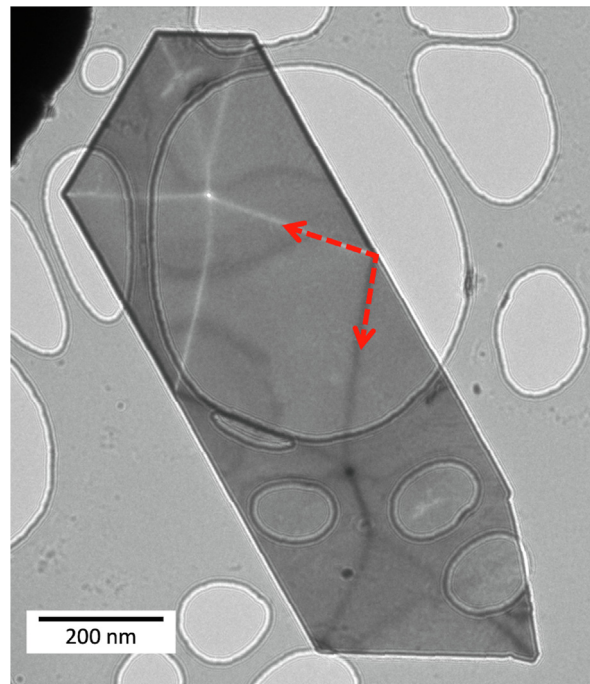

Fig. 7. Lorentz microscope image (2 mm under-focus) of a Co platelet with closure multi-domain structure. The bright and dark lines are the domain walls, and are highlighted by the red dashed lines. (For interpretation of the references to color in this figure legend, the reader is referred to the web version of this article.)
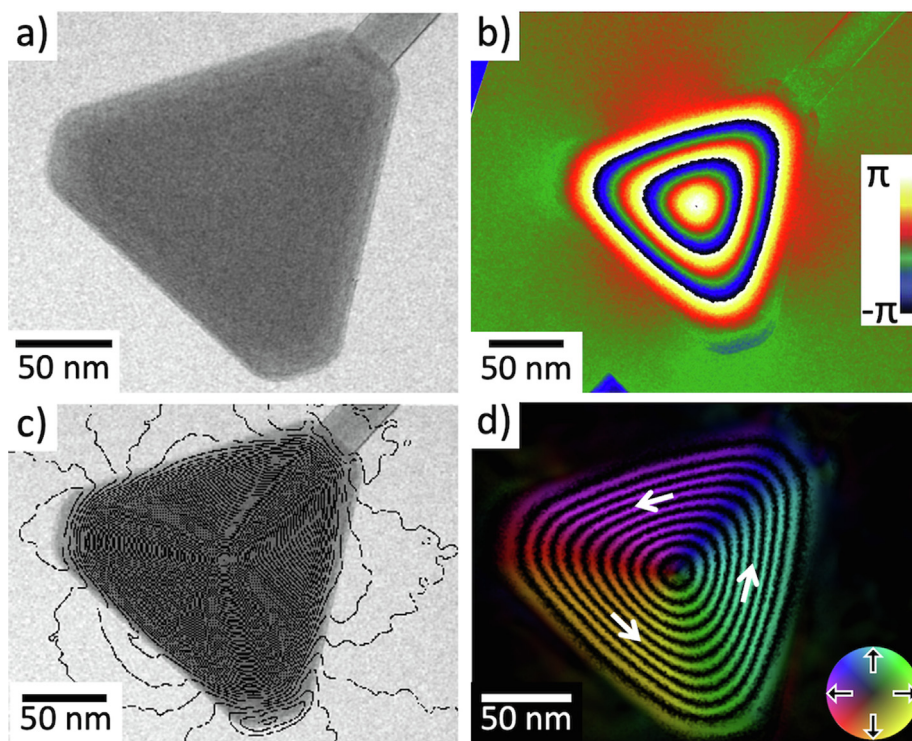

Fig. 6. Electron holography results of a Co platelet: (a) amplitude image; (b) MAG phase shift; (c) MAG phase contour overlaid with the amplitude image showing the in plane magnetic induction, the spacing of the contour is 0.21 rad; (d) Magnetic flux lines calculated as the cosine of 4 times the MAG contribution to the measured phase shift. A low pass filter was applied to suppress the high frequency noise. The direction of the measured magnetic induction is indicated according to the color wheel and the magnetization direction of the whisker is pointed out by the white arrow.

multi-domain structure with its domain walls (bright and dark lines) highlighted by the red dashed lines. The dimension of the platelet is very different from that of a whisker. The width of the platelet is 400 ± 10 nm, its length is 1.2 ± 0.02 µm. It seems that, unlike whiskers, the single domain structure is not favored for platelets with large surface area and small aspect ratio, nor is the vortex state if the platelet is not highly symmetric, the most stable state in this case is thus the closure multi domain structure.

4. Conclusion

In conclusion, Fe and Co nano-whiskers and platelets were successfully synthesized. Both platelets and whiskers are freestanding with well-defined microstructure. The surfaces are low index crystal planes, with their cross section dominated by the Wulff shape. The Fe whiskers were found to be of BCC crystal structure, single crystalline and defect-scarce. In contrast, both FCC and HCP structures were observed in Co whiskers. Stacking faults and microtwins are often observed in Co whiskers. The magnetocrystalline easy axis of BCC α-Fe is parallel to the Fe whisker axis. For Co whiskers, neither the FCC nor the HCP easy magnetization axis is parallel to their whisker axis. Changes in defect density did not influence the magnetization direction. Remarkably, both Fe and Co whiskers synthesized in this work were all single domain structures with magnetization along the whisker axis. The magnetization direction was dictated by the predominating shape anisotropy (rather than the magnetocrystalline anisotropy), as a result of the high aspect ratio of the whiskers. Vortex state was observed in highly symmetric small platelets. Larger platelets with lower level of symmetry, on the other hand, exhibited a multi-domain structure, but still exhibiting low indexed surface planes. The result paves way for the fabrication of high-quality core–shell or layered structures. The perfect surfaces of the nano-whiskers and platelets allow for homogeneous and position invariant nucleation of a second phase, retaining the defect-scarceness in subsequently grown shell or layers.

Declaration of Competing Interest

The authors declare that they have no known competing financial interests or personal relationships that could have appeared to influence the work reported in this paper.

References

[1] Y. Hanaoka, K. Hinode, K. Takeda, D. Kodama, Increase in electrical resistivity of copper and aluminum fine lines, Mater. Trans. 43 (2002) 1621–1623, https://doi.org/10.2320/matertrans.43.1621.

[2] W.D. Nix, Mechanical properties of thin films, Metall. Trans. A. 20 (1989) 2217–2245, https://doi.org/10.1007/BF02666659.

[3] G. Richter, K. Hillerich, D.S. Gianola, R. Mönig, O. Kraft, C. a Volkert, Ultrahigh strength single crystalline nanowhiskers grown by physical vapor deposition, Nano Lett. 9 (2009) 3048–3052, https://doi.org/10.1021/nl9015107.

[4] L. Weissmayer, Keimbildung und Wachstum metallischer Whisker, University Stuttgart, 2013.

[5] S. Patel, H. Park, P. Bonato, L. Chan, M. Rodgers, A review of wearable sensors and systems with application in rehabilitation, J. Neuroeng. Rehabil. 9 (2012) 1–17, https://doi.org/10.1186/1743-0003-9-21.

[6] J. Zhou, Y. Gu, P. Fei, W. Mai, Y. Gao, R. Yang, G. Bao, Z.L. Wang, Flexible piezotronic strain sensor, Nano Lett. 8 (2008) 3035–3040, https://doi.org/10.1021/nl802367t.

[7] W. Jing, X. Chen, S. Lyttle, Z. Fu, Y. Shi, D.J. Cappelleri, A magnetic thin film microrobot with two operating modes, in: Proc. - IEEE Int. Conf. Robot. Autom., 2011, pp. 96–101. https://doi.org/10.1109/ICRA.2011.5980072.

[8] A. Ghost, P. Fischer, Controlled propulsion of artificial magnetic nanostructured propellers, Nano Lett. 9 (2009) 2243–2245, https://doi.org/10.1021/nl900186w.

[9] S.S. Brenner, The growth of whiskers by the reduction of metal salts, Acta Metall. 4 (1956) 62–74, https://doi.org/10.1016/0001-6160(56)90111-0.

[10] R.W. DeBlois, C.D. Graham, Domain observations on iron whiskers, J. Appl. Phys. 29 (1958) 528–529, https://doi.org/10.1063/1.1723210.

[11] H.R. Khan, K. Petrikowski, Structural Magnetic Properties of the Electrochemically Deposited Arrays of Nickel Nanowires, MRS Proc. 581 (1999) 245, https://doi.org/10.1557/PROC-581-245.

[12] H. Schlörb, V. Haehnel, M.S. Khatri, A. Srivastav, A. Kumar, L. Schultz, S. Fähler, Magnetic nanowires by electrodeposition within templates, Phys. Status Solidi. 247 (2010) 2364–2379, https://doi.org/10.1002/pssb.201046189.

[13] L. Mohaddes-Ardabili, H. Zheng, S.B. Ogale, B. Hannoyer, W. Tian, J. Wang, S.E. Lofland, S.R. Shinde, T. Zhao, Y. Jia, L. Salamanca-Riba, D.G. Schlom, M. Wuttig, R. Ramesh, Self-assembled single-crystal ferromagnetic iron nanowires formed by decomposition, Nat. Mater. 3 (2004) 533–538, https://doi.org/10.1038/nmat1162.

[14] H. Schumann, G. Richter, A. Leineweber, Crystallography of γ′-Fe4N formation in single-crystalline α-Fe whiskers, J. Appl. Crystallogr. 53 (2020) 865–879, https://doi.org/10.1107/S1600576720005981.

[15] A. Fert, L. Piraux, Magnetic nanowires, J. Magn. Magn. Mater. 200 (1999) 338–358, https://doi.org/10.1016/S0304-8853(99)00375-3.

[16] C. Neetzel, T. Ohgai, T. Yanai, M. Nakano, H. Fukunaga, Uniaxial Magnetization Performance of Textured Fe Nanowire Arrays Electrodeposited by a Pulsed Potential Deposition Technique, Nanoscale Res. Lett. 12 (2017) 1–8, https://doi.org/10.1186/s11671-017-2367-3.

[17] M.S. Gudiksen, L.J. Lauhon, J. Wang, D.C. Smith, C.M. Lieber, Growth of nanowire superlattice structures for nanoscale photonics and electronics, Nature. 415 (2002) 617–620, https://doi.org/10.1038/415617a.

[18] L.J. Lauhon, M.S. Gudiksen, C.L. Wang, C.M. Lieber, Epitaxial core-shell and core-multishell nanowire heterostructures, Nature. 420 (2002) 57–61, https://doi.org/10.1038/nature01141.

[19] C.M. Lieber, Z.L. Wang, Functional Nanowires, MRS Bull. 32 (2007) 99–108, https://doi.org/10.1557/mrs2007.41.

[20] A. Sedlmayr, E. Bitzek, D.S. Gianola, G. Richter, R. Mönig, O. Kraft, Existence of two twinning-mediated plastic deformation modes in Au nanowhiskers, Acta Mater. 60 (2012) 3985–3993, https://doi.org/10.1016/j.actamat.2012.03.018.

[21] S. Baylan, G. Richter, M. Beregovsky, D. Amram, E. Rabkin, The kinetics of hollowing of Ag-Au core-hell nanowhiskers controlled by short-circuit diffusion, Acta Mater. 82 (2015) 145–154, https://doi.org/10.1016/j.actamat.2014.08.057.

[22] B. Roos, B. Kapelle, G. Richter, C.A. Volkert, Surface dislocation nucleation controlled deformation of Au nanowires, Appl. Phys. Lett. 105 (2014), https://doi.org/10.1063/1.4902313.

[23] G. Richter, Fabrication of freestanding gold nanotubes, Scr. Mater. 63 (2010) 933–936, https://doi.org/10.1016/j.scriptamat.2010.07.007.

[24] L. Landau, E. Lifshitz, On the Theory of the Dispersion of Magnetic Permeability in Ferromagnetic Bodies, Phys. Zeitsch. Der Sow. 169 (1935) 153–169.

[25] C. Kittel, Theory of the structure of ferromagnetic domains in films and small particles, Phys. Rev. 70 (1946) 965–971, https://doi.org/10.1103/PhysRev.70.965.

[26] C.Z. Li, J.C. Lodder, The influence of the packing density on the magnetic behaviour of alumite media, J. Magn. Magn. Mater. 88 (1990) 236–246, https://doi.org/10.1016/S0304-8853(97)90033-0.

[27] D.S. Choi, J. Park, S. Kim, D.H. Gracias, M.K. Cho, Y.K. Kim, A. Fung, S.E. Lee, Y. Chen, S. Khanal, S. Baral, J.H. Kim, Hyperthermia with magnetic nanowires for inactivating living cells, J. Nanosci. Nanotechnol. 8 (2008) 2323–2327, https://doi.org/10.1166/jnn.2008.273.

[28] K.K. Mehta, T.H. Wu, E.P.Y. Chiou, Magnetic nanowire-enhanced optomagnetic tweezers, Appl. Phys. Lett. 93 (2008), https://doi.org/10.1063/1.3050520 254102.

[29] J.M. Park, S.J. Kim, J.H. Jang, Z. Wang, P.G. Kim, D.J. Yoon, J. Kim, G. Hansen, K.L. DeVries, Actuation of electrochemical, electro-magnetic, and electro-active actuators for carbon nanofiber and Ni nanowire reinforced polymer composites, Compos. Part B Eng. 39 (2008) 1161–1169, https://doi.org/10.1016/j.compositesb.2008.03.009.

[30] R.W. DeBlois, C.P. Bean, Nucleation of Ferromagnetic Domains in Iron Whiskers, J. Appl. Phys. 30 (1959) S225, https://doi.org/10.1063/1.2185899.

[31] C. Kittel, Physical Theory of Ferromagnetic Domains, Rev. Mod. Phys. 21 (1949) 541–583, https://doi.org/10.1103/RevModPhys.21.541.

[32] A. Hubert, Rudolf Schäfer, Magnetic Domains (1998), https://doi.org/10.1007/978-3-540-85054-0.

[33] G.L. Kellogg, The mobility and structure of nickel atoms on the (100) plane of tungsten, Surf. Sci. Lett. 192 (1987) L879–L886, https://doi.org/10.1016/0167-2584(87)90790-0.

[34] Y.G. Zhou, X.T. Zu, J.L. Nie, H.Y. Xiao, First-principles study of Ni adsorption on Mo (110), Surf. Rev. Lett. 15 (2008) 661–668, https://doi.org/10.1142/S0218625X08011822.

[35] L. Vitos, A.V. Ruban, H.L. Skriver, J. Kollár, The surface energy of metals, Surf. Sci. 411 (1998) 186–202, https://doi.org/10.1016/S0039-6028(98)00363-X.

[36] J.B. Wagner, K.R. Lawless, A.T. Gwathmey, The Rates of Formation and Structure of Oxide Films Formed on A Single Crystal of Iron, Trans. Metall. Soc. AIME. 221 (1961) 257–261.

[37] C. Stockbridge, P. Sewell, M. Cohen, Cathodic Behavior of Iron Single Crystals and the Oxides Fe3O4, Gamma-Fe2O3, and Alpha-Fe2O3, J. Electrochem. Soc. 108 (1961) 928–933, https://doi.org/10.1149/1.2427923.

[38] F.E. Luborsky, E.F. Koch, C.R. Morelock, Crystallographic Orientation and Oxidation of Submicron Whiskers of Iron, Iron-Cobalt, and Cobalt, J. Appl. Phys. 34 (1963) 2905, https://doi.org/10.1063/1.1729829.

[39] B.D. Cullity, C.D. Graham, Introduction to Magnetic Materials, second ed., John Wiley & Sons, 2008. https://doi.org/10.1002/9780470386323.

[40] H. Kronmüller, M. Fähnle, Micromagnetism and the Microstructure of Ferromagnetic Solids, Cambridge University Press, 2003.

[41] A. Aharoni, Demagnetizing factors for rectangular ferromagnetic prisms, J. Appl. Phys. 83 (1998) 3432–3434, https://doi.org/10.1063/1.367113.

[42] C.A.F. Vaz, J.A.C. Bland, G. Lauhoff, Magnetism in ultrathin film structures, Reports Prog. Phys. 71 (2008), https://doi.org/10.1088/0034-4885/71/5/056501 056501.

[43] H.P. Myers, W. Sucksmith, The spontaneous magnetization of cobalt, Proc. R. Soc. London. Ser. A. Math. Phys. Sci. 207 (1951) 427–446, https://doi.org/10.1098/rspa.1951.0132.

[44] J. Crangle, LIX. The magnetic moments of cobalt-copper alloys, London, Edinburgh, Dublin Philos, Mag. J. Sci. (1955), https://doi.org/10.1080/14786440508520586.

[45] D. Weller, G.R. Harp, R.F.C. Farrow, A. Cebollada, J. Sticht, Orientation Dependence of the Polar Kerr Effect in fcc and hcp Co, Phys. Rev. Lett. 72 (1994) 2097–2100, https://doi.org/10.1103/PhysRevLett.72.2097.

[46] R.P. Cowburn, Property variation with shape in magnetic nanoelements, J. Phys. D. Appl. Phys. 33 (2000) R1–R16, https://doi.org/10.1088/0022-3727/33/1/201.